Ping Wang,[1] Byunghee Yoo,[1] Jingsheng Yang,[2] Xueli Zhang,[1,3] Alana Ross,[1] Pamela Pantazopoulos,[1] Guangping Dai,[2] and Anna Moore[1]

GLP-1R–Targeting Magnetic Nanoparticles for Pancreatic Islet Imaging

Diabetes 2014;63:1465–1474 | DOI: 10.2337/db13-1543

Noninvasive assessment of pancreatic β-cell mass would tremendously aid in managing type 1 diabetes (T1D). Toward this goal, we synthesized an exendin-4 conjugated magnetic iron oxide–based nanoparticle probe targeting glucagon-like peptide 1 receptor (GLP-1R), which is highly expressed on the surface of pancreatic β-cells. In vitro studies in βTC-6, the β-cell line, showed specific accumulation of the targeted probe (termed MN-Ex10-Cy5.5) compared with nontargeted (termed MN-Cy5.5). In vivo magnetic resonance imaging showed a significant transverse relaxation time (T2) shortening in the pancreata of mice injected with the MN-Ex10-Cy5.5 probe compared with control animals injected with the nontargeted probe at 7.5 and 24 h after injection. Furthermore, ΔT2 of the pancreata of prediabetic NOD mice was significantly higher than that of diabetic NOD mice after the injection of MN-Ex10-Cy5.5, indicating the decrease of probe accumulation in these animals due to β-cell loss. Of note, ΔT2 of prediabetic and diabetic NOD mice injected with MN-Cy5.5 was not significantly changed, reflecting the nonspecific mode of accumulation of nontargeted probe. We believe our results point to the potential for using this agent for monitoring the disease development and response of T1D to therapy.

Diabetes, a metabolic disorder, results from an inadequate mass of functional β-cells. In type 1 diabetes (T1D), β-cells are destroyed by the immune system. Type 2 diabetes (T2D) is associated with insulin resistance and β-cell dysfunction (1). The reduction in β-cell mass is a common feature of both T1D and T2D (2). Although monitoring autoantibody titers and C-peptide concentrations could provide useful information for diabetes treatment (3), a noninvasive method of directly monitoring the disease progression by quantifying β-cell mass and/or function would provide unprecedented advantages for disease treatment. Various imaging methods allowing for β-cell visualization have been developed (4). However, despite intense research efforts, only one tracer (dihydrotetrabenazine) for positron emission tomography has been developed and is currently under clinical evaluation (5). Therefore, there is an urgent need to develop an imaging probe that would enable simple, reproducible, and safe in vivo imaging of islet β-cells.

Glucagon-like peptide 1 (GLP-1) is a peptide hormone synthesized in the small intestine in response to nutrient ingestion. GLP-1 binds to the GLP-1 receptor (GLP-1R), which is expressed on islet β-cells and belongs to a G protein–coupled receptor family. Among the functional effects of GLP-1 in pancreatic islet β-cells are augmentation of glucose-induced insulin secretion, upregulation of insulin biosynthesis, and antiapoptotic influences of pancreatic β-cells, known as the "incretin effect." GLP-1R agonists have been considered for diabetes therapy, which was firstly demonstrated in proof-of-concept studies that included administration of GLP-1 to T2D patients (6,7). Because of its short biological half-life due to pipeptidyl

[1]Molecular Imaging Laboratory, Massachusetts General Hospital/Massachusetts Institute of Technology/Harvard Medical School Athinoula A. Martinos Center for Biomedical Imaging, Department of Radiology, Massachusetts General Hospital, Harvard Medical School, Boston, MA
[2]Massachusetts General Hospital/Massachusetts Institute of Technology/Harvard Medical School Athinoula A. Martinos Center for Biomedical Imaging, Department of Radiology, Massachusetts General Hospital, Harvard Medical School, Boston, MA
[3]Center for Drug Discovery, School of Pharmacy, China Pharmaceutical University, Nanjing, China

Corresponding author: Anna Moore, amoore@helix.mgh.harvard.edu.

Received 7 October 2013 and accepted 19 January 2014.

This article contains Supplementary Data online at http://diabetes.diabetesjournals.org/lookup/suppl/doi:10.2337/db13-1543/-/DC1.

peptidase IV (DPP IV) cleavage, long-acting analogs have been developed. Exendin-4, a GLP-1R agonist and GLP-1 analog resistant to DPP IV (8), displays biological properties similar to human GLP-1, with which it shares 53% sequence identity. Because of GLP-1R specific expression on β-cells, GLP-1 and its analogs have been proposed as targeting ligands for imaging. As such, exendin-4 derivatives have been tested for fluorescence imaging or nuclear imaging of endogenous β-cells (1,9–12), transplanted islets (13–15), and insulinomas (16–22).

Compared with fluorescence and nuclear imaging modalities, magnetic resonance imaging (MRI) has certain advantages, which include high spatial resolution, true tomographic capabilities, ease of clinical translation, and the absence of ionizing radiation. Furthermore, MRI probes could be used as theranostic agents that deliver diagnostic imaging probes and therapeutics at the same time. We see the application of theranostics for diabetes treatment as an ultimate goal of our research.

The first step in designing agents with image-guided capabilities is to identify a targeting component that directs the imaging probe to the tissue of interest. For targeting pancreatic β-cells, we used as an MRI contrast agent iron oxide–based magnetic nanoparticles (MN) conjugated to exendin-4 (targeting ligand). In the current study, we describe the synthesis, characterization, and testing of magnetic conjugates that mediate their accumulation in pancreatic β-cells through receptor-mediated endocytosis (23,24). The results of our studies demonstrated preferential uptake of the MN–exendin-4 conjugate by a β-cell cell line in vitro and by pancreatic β-cells in vivo after an intravenous injection. Furthermore, accumulation of this probe in the pancreas of diabetic NOD mice was significantly reduced, as reflected by the changes of transverse relaxation time (ΔT2) on MRIs, presumably due to reduced β-cell mass in these animals. We believe our findings will serve as a building block in creating a theranostic approach for treating the diabetic pancreas.

RESEARCH DESIGN AND METHODS

Animals, Cells Lines, and Mouse Islet Isolation

All animal experiments were performed in compliance with institutional guidelines and approved by the Massachusetts General Hospital (MGH) Institutional Animal Care and Use Committee. Female mice (Balb/c, 6–10 weeks old; A/J, 10 weeks old; and NOD, 5 and 15 weeks old) were purchased from The Jackson Laboratories (Bar Harbor, ME). Mice with a serum glucose concentration above 250 mg/dL on two consecutive measurements were considered diabetic.

The mouse insulinoma β-cell line βTC6, purchased from American Type Culture Collection (Manassas, VA), was grown in Dulbecco's modified Eagle's medium supplemented with 15% (vol/vol) FBS and 1% penicillin-streptomycin. The mouse pancreatic ductal adenocarcinoma cell line Ptf1-Cre (non–β-cell line; a gift from Dr. Nabeel Bardeesy, MGH) was used as the control. GLP-1R expression in pancreatic islets has been shown previously (25). To use βTC6 cells for targeting, we confirmed GLP-1R expression in these cells by staining with rabbit anti–GLP-1R antibody (Abcam, Cambridge, MA), followed by fluorescein isothiocyanate (FITC)-conjugated anti-rabbit IgG (H+L) secondary antibody (Vector Laboratories, Burlingame, CA). After incubation, cover slips were mounted with DAPI-containing mounting medium (Vectashield; Vector Laboratories). GLP-1R expression was clearly visualized using fluorescence microscopy (Eclipse 50i; Nikon Metrology, Brighton, MI) (Supplementary Fig. 1).

Murine islets were isolated by collagenase P (Roche Applied Science, Indianapolis, IN) digestion (26), followed by purification using Histopaque-1077 (Sigma-Aldrich, St. Louis, MO) density centrifugation, as described (27). Islets were cultured in CMRL-1066 medium (Gibco, Grand Island, NY) supplemented with 10% FBS and 1% penicillin-streptomycin.

Probe Synthesis and Characterization

In this current project, we synthesized a nanoparticle probe carrying exendin-4 for selective targeting of pancreatic β-cells. Briefly, the N-terminus of exendin-4 (1 mg, 239 nmol; AnaSpec, Inc., San Jose, CA) was protected by the Fmoc group through the conjugation with Fmoc-NHS (121 μg in 100 μL DMSO, 1.5 equiv.) in PBS (50 mmol/L, pH 6.5) for 24 h. To introduce the thiol group, N-succinimidyl-S-acetylthioacetate hydrochloride (SATA; 0.11 mg, 2 equiv.), after deacetylation by hydroxylamine, was introduced to the side chain of lysine in Fmoc-protected exendin-4 in PBS buffer (pH 8.5) for 24 h. The Fmoc group was then deprotected by 20% piperidine in dimethylformamide for 30 min. Exendin-4 derivatives in each step were purified by high-performance liquid chromatography–photo-diode array. Iron oxide nanoparticles were synthesized in our laboratory, as described previously (28), and labeled with Cy5.5 (Amersham Biosciences, Piscataway, NJ), followed by modification with N-[γ-maleimidobutyryloxy] succinimide ester (GMBS). SATA-conjugated exendin-4 was loaded on GMBS-modified iron nanoparticles through thioether formation. Surface modified MNs were purified by size exclusion column (PD-10, GE Healthcare) in each conjugation step. Conjugated nanoparticles were termed MN-Ex5-Cy5.5 or MN-Ex10-Cy5.5, reflecting the number of exendin-4 molecules per nanoparticle.

The size of the conjugated nanoparticles was measured using dynamic light scattering (Zetasizer Nano ZS; Malvern Instruments Ltd., Worcestershire, U.K.). Nanoparticle relaxivity was measured using a 20-MHz nuclear MR spectrometer (Bruker MiniSpec). The nontargeted control MN-Cy5.5 probe was synthesized and characterized as well.

In Vitro Cell Viability, Insulin Secretion, Uptake, and Competitive Inhibition Assays

Cell viability was determined by colorimetric assay using the CellTiter 96 nonradioactive cell proliferation assay kit (Promega, Madison, WI) according to the manufacturer's

manual. Cells were seeded into 96-well plates and incubated with experimental and control probes for 3 h, followed by addition of a tetrazolium dye solution. After overnight incubation with solubilization solution/stop mix, the plate was read on a SpectraMax M2 spectrophotometer (λ test = 570 nm; Molecular Devices, Sunnyvale, CA).

Glucose-stimulated insulin secretion in βTC-6 cells was evaluated using a rodent insulin ELISA kit (Mercodia, Uppsala, Sweden) according to the manufacturer's instructions. Cells were seeded into 12-well plates (2×10^5/well) and incubated with MN-Ex10-Cy5.5 or with control probes (50 μg iron/well) at low (1.7 mmol/L) and high (20 mmol/L) glucose concentrations. Insulin concentrations in supernatants and the insulin content in cells were measured. A stimulation index was calculated as the ratio of glucose-stimulated insulin secretion to basal insulin secretion normalized by the insulin content (29,30).

For the uptake assay, two cell lines were seeded into 96-well plates and incubated with MN-Ex5-Cy5.5 and MN-Ex10-Cy5.5 at various concentrations for 1.5 or 3 h at 37°C. After incubation, fluorescence levels were measured using the IVIS Spectrum imaging system (PerkinElmer/Caliper LifeSciences, Hopkinton, MA), at λ_{ex} = 675 nm and λ_{em} = 720 nm, and normalized to total cell protein determined by bicinchoninic acid protein assay (Pierce, Thermo Fisher Scientific, Inc., Rockford, IL).

For competitive inhibition assay, cell lines were seeded into 96-well plates and incubated with MN-Ex10-Cy5.5 (50 μg iron/well) for 1.5 h alone or with increasing doses of exendin-4 (0–4,330 nmol/L) added 1 h before incubation with the probe. After incubation, cells were washed three times with PBS, and fluorescence intensities were read and normalized to total cell protein, as described above.

Fluorescence microscopy was performed using βTC-6 cells or isolated murine islets after incubation with MN-Ex10-Cy5.5 probe. Additional confirmation of probe accumulation in βTC-6 cells was obtained by fluorescence microscopy by colocalizing the Cy5.5 signal from the probe with the staining for GLP-1R, as described above.

Biodistribution Studies

For biodistribution studies, MN-Ex10-Cy5.5 or control MN-Cy5.5 probe (10 mg Fe/kg) was injected intravenously in Balb/c mice (n = six). Ex vivo fluorescence images of isolated organs were obtained 7.5 or 24 h after intravenous probe injection. Spleen, kidney, liver, lung, heart, intestine, muscle, brain, and pancreas were excised, scanned, and analyzed using an IVIS Spectrum animal imaging system (PerkinElmer/Caliper LifeSciences). Image analysis was conducted using LivingImage 4.2 software (PerkinElmer/Caliper LifeSciences). To evaluate imaging results, a region of interest (ROI) was drawn around the selected tissue. Average signal efficiency, which is defined as fluorescence emission normalized to the incident excitation intensity (radiance of the subject/illumination intensity), was used for quantification. Data were also normalized to the organ weights.

Ex Vivo MRI of Pancreatic Tissue From Healthy Mice

Six-week-old Balb/c mice were injected intravenously with MN-Ex10-Cy5.5 or with control MN-Cy5.5 probe (10 mg Fe/kg, n = four in each group) and sacrificed 7.5 or 24 h after injection. The pancreatic tissues were excised and fixed for ex vivo MRI performed using a Magnex/Agilent 13-cm horizontal bore scanner operating at 15 T interfaced to a Siemens clinical MR console. T2 maps were acquired (pulse sequences are described in detail in the Supplementary Materials). T2 maps were analyzed voxel-by-voxel by fitting the T2 measurements to a standard exponential decay curve, defined by the following equation: $[y = A^{(-t/T2)}]$. T2 times in ROIs surrounding the pancreas were calculated using Marevisi 3.5 software (Institute for Biodiagnostics, National Research Council Canada).

In Vivo MRI of Pancreata in Healthy and Diabetic Mice

To evaluate probe accumulation in vivo, we performed MRI in healthy and diabetic mice. Six-week-old Balb/c mice and 10-week-old A/J mice were intravenously injected with MN-Ex10-Cy5.5 or with control MN-Cy5.5 probe (10 mg Fe/kg, n = six in each group). In vivo MRI was performed 1.5, 3, 7.5, and 24 h later using a 9.4T Bruker horizontal bore scanner equipped with a home-built radio frequency transmit and receive 3×4 cm elliptical surface coils. The imaging protocol consisted of multislice multiecho T2-weighted map and T2*-weighted three-dimensional (3D) sequences (described in detail in the Supplementary Materials). T2 map images were analyzed using a similar procedure described above. Two investigators blinded to sample identity analyzed the obtained results independently. Female NOD mice (5-week-old prediabetic and 15-week-old diabetic, n = three in each group) were imaged before and 7.5 h after an intravenous injection of MN-Ex10-Cy5.5 or MN-Cy5.5. T2 relaxation times derived from ROIs surrounding the pancreas were analyzed as described above. ΔT2 was calculated according to the equation $\Delta T2 = (T2_{preinjection} - T2_{postinjection})$.

Ex Vivo Histology, Immunostaining, and Fluorescence Microscopy

Histology was performed on pancreatic frozen sections from healthy mice by staining for insulin and colocalizing it with Cy5.5 signal derived from the probe 1.5, 7.5, and 24 h after injection. Sections were stained with anti-insulin antibody (Santa Cruz Biotechnology, Santa Cruz, CA), followed by incubation with FITC-labeled secondary goat anti-rabbit IgG (Vector Laboratories, Inc., Burlingame, CA) and counterstained with DAPI (Vectashield; Vector Laboratories). Pancreatic frozen sections from prediabetic and diabetic NOD mice were also stained using anti–GLP-1R antibody (Abcam) or anti-insulin antibody (Santa Cruz Biotechnology) and colocalized with Cy5.5 signal. Observers blinded to the treatments evaluated all tissue sections.

Statistical Analysis

Data are presented as mean ± SD. Statistical comparisons between two groups were evaluated by Student *t* test and corrected by the repeated two-way ANOVA for the time course analysis using GraphPad Prism 5 software (GraphPad Software, Inc., La Jolla, CA). A value of $P < 0.05$ was considered statistically significant.

RESULTS

Characterizations of the Probes

A schematic representation of GLP-1R-specific probes is shown in Supplementary Fig. 2. Exendin-4 was conjugated to iron nanoparticles using the side chain of Lys27, which was the dominant reaction site on the peptide for conjugation to nanoparticles. The second potential reaction site on Lys12 side chain is hindered and could not serve as the major reaction site (31,32). The ratio of Cy5.5:exendin-4:nanoparticles was determined as 2.5:5:1 or 2.5:10:1 by spectrophotometric analysis and bicinchoninic acid protein assay. The core size of the control probe was 22.31 ± 0.54 nm, whereas the core size of the exendin-4–conjugated nanoparticles was 32.65 ± 1.09 nm. R2 relaxivity determined at 20 MHz was 103.04 $mmol/L^{-1} \cdot s^{-1}$.

Cell Viability, Insulin Secretion, Probe Uptake, and Competition Inhibition Assay

To evaluate toxicity associated with the probes, we performed a 3-(4,5-dimethylthiazol-2-yl)-2,5-diphenyltetrazolium bromide (MTT) assay on βTC-6 cells incubated with different concentrations of the probes. The results showed that treatment with the probes did not have any significant effect on cell viability in vitro (Supplementary Fig. 3). The insulin-secretion assay showed that the presence of exendin-4 on the nanoparticles did not change glucose-stimulated insulin secretion in the β-cell line as charged by the stimulation index (Supplementary Fig. 4). Our in vitro studies also demonstrated a concentration-dependent uptake of MN–exendin-4 conjugated probes by βTC-6 cells and a background signal with control MN-Cy5.5 probe. The uptake of the probe that contained 10 exendin-4 molecules/nanoparticle showed higher accumulation and was therefore selected for subsequent in vivo studies. The intensity of a background signal observed in control Ptf1-Cre ductal pancreatic carcinoma cells was an order of magnitude lower than in the β-cell line (Fig. 1*A*). A competition assay using free exendin-4 peptide as a blocking agent showed specific binding to βTC-6 cells and no competition with control cells (Fig. 1*B*). Concentration-dependent internalization of the probe in the βTC-6 cells and intact murine islets was confirmed by fluorescence microscopy (Fig. 1*C* and *D*) and showed colocalization with GLP-1R (Supplementary Fig. 5).

Biodistribution of Systemically Delivered MN-Ex10-Cy5.5 Probe

Biodistribution study in vivo was performed in BALB/c mice after an intravenous injection of the MN-Ex10-Cy5.5 or control probe. We observed preferential accumulation of the MN-Ex10-Cy5.5 probe in the pancreas at 24 h after injection compared with the control probe (Fig. 2 and Supplementary Fig. 6). The higher accumulation of both probes in the pancreas at 7.5 h after injection compared with the accumulation at 24 h reflects the persistence of long-circulated nanoparticles in the blood pool at this earlier time and is in accordance with their known kinetics (33). Prototype nanoparticles (~5% injected dose/g) have been shown to be excreted by the urinary and fecal route at 7.5 h (33). Note that the accumulation of the MN-Ex10-Cy5.5 probe was overall higher than that of the control probe at 24 h but did not reach statistical significance using this method (Fig. 2*B* and Supplementary Fig. 6*A*). However, accumulation of MN-Ex10-Cy5.5 at 24 h was 3.29 times higher than that of the control probe (1.37×10^9 vs. 4.17×10^8 as normalized Cy5.5 fluorescence intensity), presumably due to the retention of the former and the clearance of the later (Fig. 2*C* and Supplementary Fig. 6*B* and *D*). The rest of the organs showed accumulation consistent with the literature on related iron oxide nanoparticles (34,35), which could be taken up by macrophages, mostly in liver, spleen, and lymph nodes, within 24 h after a bolus injection and undergo progressive metabolism (36). Studies showed that several other tissues, including heart, intestine, and the central nervous system, also expressed GLP-1R (37–39), which might be the reason the accumulation of the probes was also observed in other organs in our biodistribution studies. Although this would not play a role in MRI studies, it could potentially result in off-target effects if these probes were used for drug-delivery purposes.

Ex Vivo and In Vivo MRI of Murine Pancreata

Ex vivo imaging of mouse pancreata was performed on excised organs from healthy mice injected with experimental or control probes using a 15-T MRI scanner. The T2 relaxation times of the pancreatic tissues at 7.5 h or 24 h after injection are summarized in Fig. 3*A* and *B*. The results showed the significant decrease of T2 in the pancreata of the animals injected with MN-Ex10-Cy5.5 at both time points compared with pancreatic tissues from the animals injected with the control probe.

Next, we performed experiments demonstrating that the MN-Ex10-Cy5.5 probe could be used for in vivo imaging of pancreatic β-cells. Quantitative analysis of T2 relaxation times of the pancreata of mice intravenously injected with the MN-Ex10-Cy5.5 or control probe showed that a drop occurred in T2 of the pancreata starting at 1.5 h after injection in both groups. In the control group, the drop was most pronounced between 1.5 and 3 h after injection, followed by a gradual T2 increase, consistent with contrast agent washout. In the MN-Ex10-Cy5.5 group, the drop reached its lowest point at 3 h after injection. The signal remained at that level up to 7 h after injection, followed by a much slower T2 increase compared with the control group.

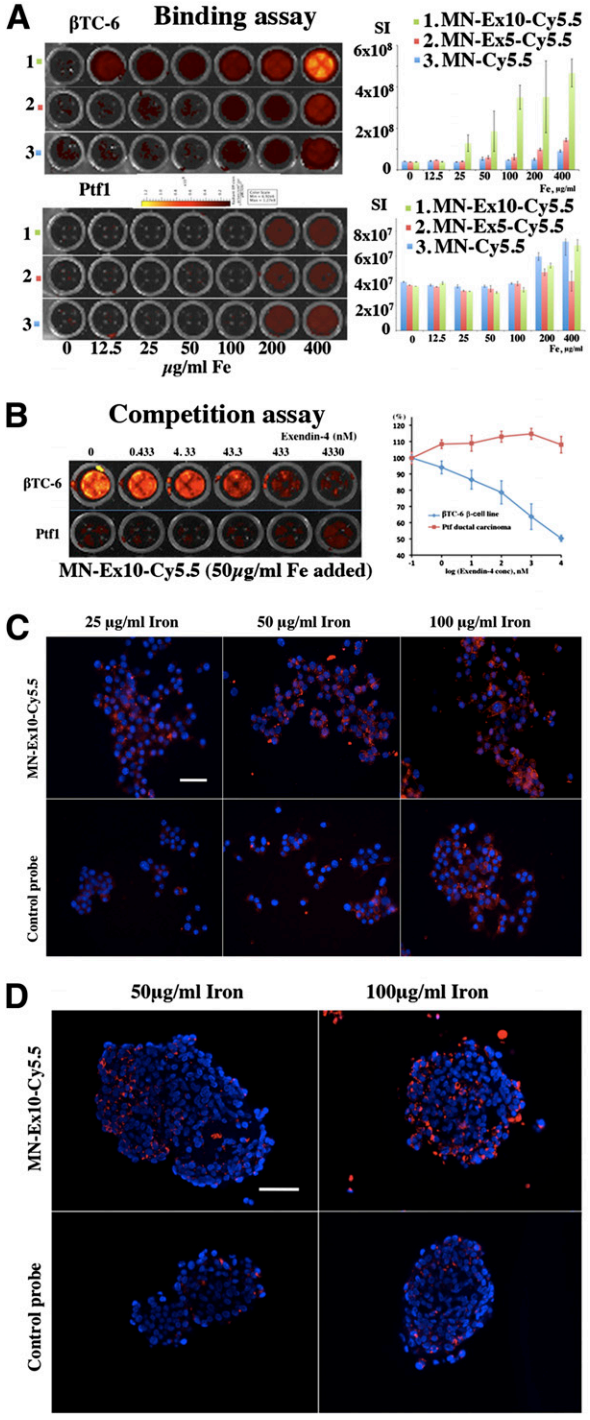

Figure 1—In vitro testing of the MN-Ex10-Cy5.5 probe. *A*: Cell-binding assays showed concentration-dependent preferential uptake of experimental MN-Ex5-Cy5.5 and MN-Ex10-Cy5.5 probes by the β-cell line compared with the control probe. There was no difference in uptake between the experimental and control probes by the pancreatic carcinoma cell line (control). *B*: Competition assays showed that accumulation of the experimental probes was dose-dependently blocked by free exendin-4 peptide. Fluorescence microscopy demonstrated concentration-dependent internalization of experimental probe in the βTC-6 cells (*C*) and in intact murine islets (*D*). Accumulation of the control probe was negligible in both cells and isolated islets (red, Cy5.5 dye; blue, DAPI nuclear stain). Magnification bar = 50 μm.

T2 map analysis demonstrated a significant difference in T2 of the pancreata in the animals injected with the MN-Ex10-Cy5.5 or control probes at 7.5 h (20.25 ± 2.24 ms vs. 26.42 ± 1.02 ms, respectively) and 24 h (22.45 ± 3.59 ms vs. 28.81 ± 1.31 ms, respectively) after injection, reflecting a stronger retention of the MN-Ex10-Cy5.5 probe (Fig. 3*C* and *D*). It is noteworthy that we observed a nonsignificant change in signal intensity at 7.5 h after injection by fluorescence imaging, whereas significance was achieved between two groups by MRI at the same time point. The seeming discrepancy between the two imaging modalities could be attributed to different sensitivities of these modalities. It is also possible that factors such as quenching of the fluorescent dye, limited tissue penetration of the light, the ex vivo scanning position, and surface weighting influenced optical imaging results.

To confirm the binding specificity of the MN-Ex10-Cy5.5 probe in islet cells, we performed ex vivo histological analysis of pancreatic sections removed 1.5, 7.5, and 24 h after injection. As shown in Fig. 3*E*, ex vivo histology revealed significant accumulation of MN-Ex10-Cy5.5 in pancreatic β-cells. By contrast, the Cy5.5 signal in the islets of mice injected with the control probe was negligible.

The suitability and specificity of the probe for imaging changes in β-cell mass was next demonstrated in NOD mice. We used prediabetic (5-week-old) and diabetic (15-week-old) animals injected with the MN-Ex10-Cy5.5 or MN-Cy5.5 probe. The 3D T2*-weighted MRI (Fig. 4*A* and Supplementary Movie 1) shows the area defining the pancreas that was used for analysis. Analysis of in vivo imaging data revealed a significant decrease in ΔT2 of the pancreatic area (defined as preinjection T2 − post injection T2) of 15-week-old mice compared with 5-week-old NOD mice as well as with healthy mice (Fig. 4*B*). The ΔT2 in animals injected with the MN-Ex10-Cy5.5 probe was significantly higher for both ages compared with animals injected with the control probe, pointing to the specificity of the former to the pancreatic β-cell. As expected, there was no significant difference in ΔT2 in the pancreata of the animals of both ages injected with MN-Cy5.5 probe, indicating the nonspecific nature of this accumulation.

We also performed ex vivo histological analysis of pancreatic sections from prediabeitc and diabetic NOD mice. As shown in Fig. 4*C* and *D*, ex vivo histology revealed a significant accumulation of MN-Ex10-Cy5.5 (Cy5.5 signal) in prediabetic pancreatic β-cells, as indicated by anti–GLP-1R and anti-insulin staining compared with control probe. Probe accumulation decreased in diabetic animals along with the reduction in GLP-1R and insulin staining.

DISCUSSION

The availability of pancreatic β-cell–specific imaging agents, which has been an elusive goal in the field of imaging, is of critical importance for the advancement

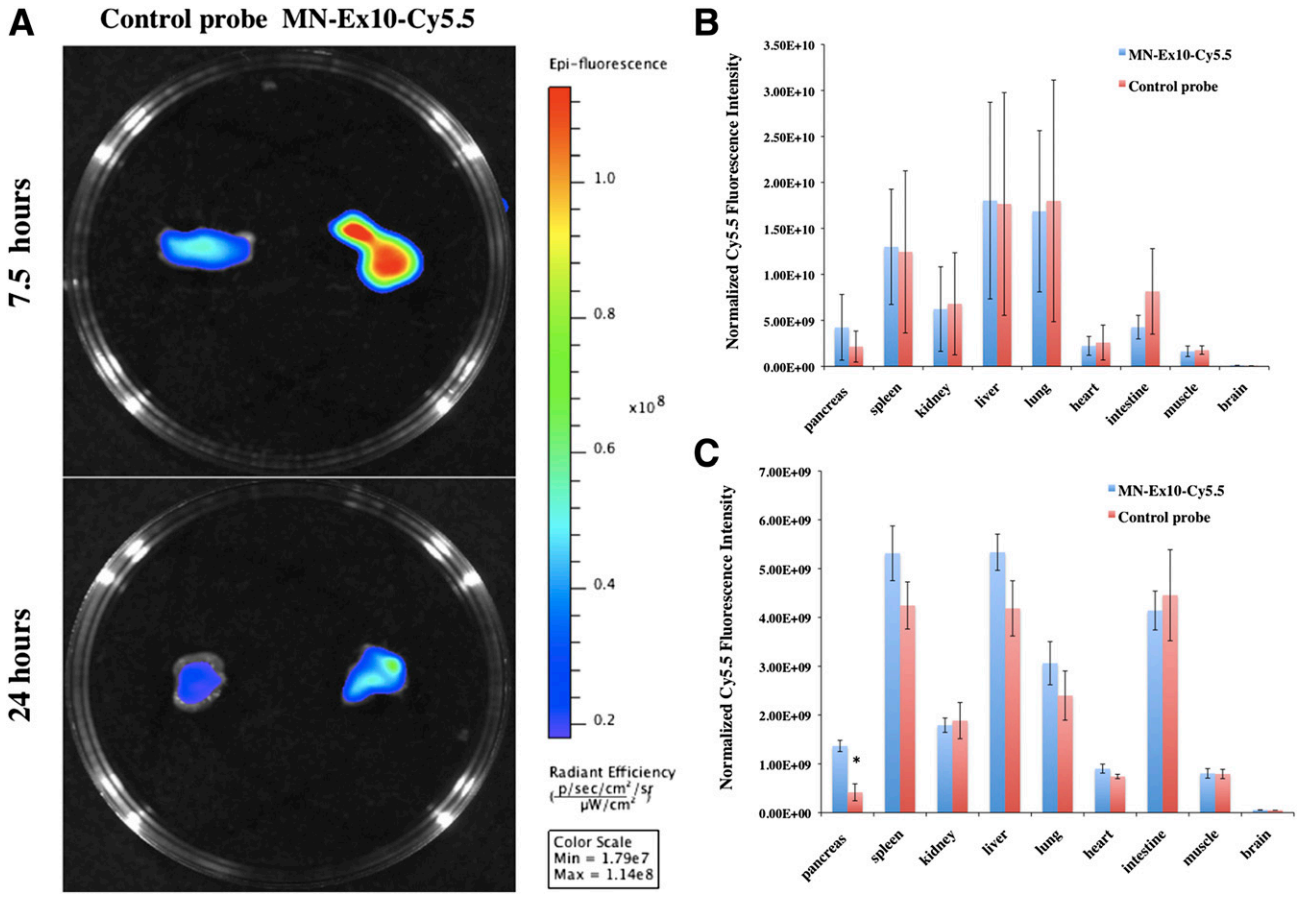

Figure 2—*A*: Ex vivo fluorescence imaging of murine pancreas at 7.5 and 24 h after an intravenous injection of MN-Ex10-Cy5.5 or control MN-Cy5.5 probes (10 mg Fe/kg). Note the higher accumulation of MN-Ex10-Cy5.5 in the pancreata of experimental animals compared with controls at both times after injection. sec, seconds. *B*: Ex vivo quantification of normalized Cy5.5 fluorescence 7.5 h after the intravenous injection of MN-Ex10-Cy5.5 and MN-Cy5.5 probes. *C*: Ex vivo quantification of normalized Cy5.5 fluorescence 24 h after the intravenous injection of MN-Ex10-Cy5.5 and MN-Cy5.5 probes. *$P < 0.05$ indicates significant difference between fluorescence intensities of pancreatic tissues of the animals injected with MN-Ex10-Cy5.5 or control probes.

of our understanding of pathophysiology and treatment of T1D (40). So far, approaches that have been explored for developing β-cell–specific MRI probes included manganese-enhanced MRI (41) and zinc-responsive gadolinium agent (42). An attempt to target GLP-1R in vivo has been limited to cancer imaging (22). Iron oxide nanoparticles targeting insulinoma in this study were not multimodal and contained a limited number of peptides conjugated to the nanoparticles through the polyethylene glycol linker, which might significantly affect their ability to be endocytosed by islet cells. Here, we report a molecularly targeted contrast agent that consists of iron oxide nanoparticles conjugated to exendin-4, which is a full agonist with high affinity and potency for the GLP-1R. The specific interaction between the GLP-1R and exendin-4 is known to induce intracellular internalization by endocytosis, which is a fundamental process used by the cells to accumulate molecules and macromolecules through deformation of the membrane and generation of membrane-bound carriers. Many nanoparticle formulations used in nanomedicine have been customized to enter cells by receptor-mediated endocytosis for cargo delivery (43). The amount of accumulated particles depends on the ligand density on the surface of the nanoparticles (44). In our current study, we synthesized iron oxide nanoparticles decorated with a different number of targeting peptide exendin-4 molecules (the molar ratio of MN to exendin-4 was 1:5 or 1:10). In agreement with ligand density dependence, the in vitro assay showed that nanoparticles with a 1:10 ratio displayed higher accumulation in target cells than nanoparticles with a 1:5 ratio. Preparation with 10 exendin-4 molecules/nanoparticle was consequentially chosen for in vivo studies.

To demonstrate specificity of the synthesized probes toward pancreatic β-cells, we performed in vivo imaging in healthy animals. Our study demonstrated a significant difference in T2 relaxation times of pancreatic tissue of experimental (injected with MN-Ex10-Cy5.5) and control (injected with MN-Cy5.5) animals, confirming target-specific accumulation of the agent. It is important to note that MRI is intrinsically a low-sensitivity technique and is not capable of resolving a single islet. In our previous

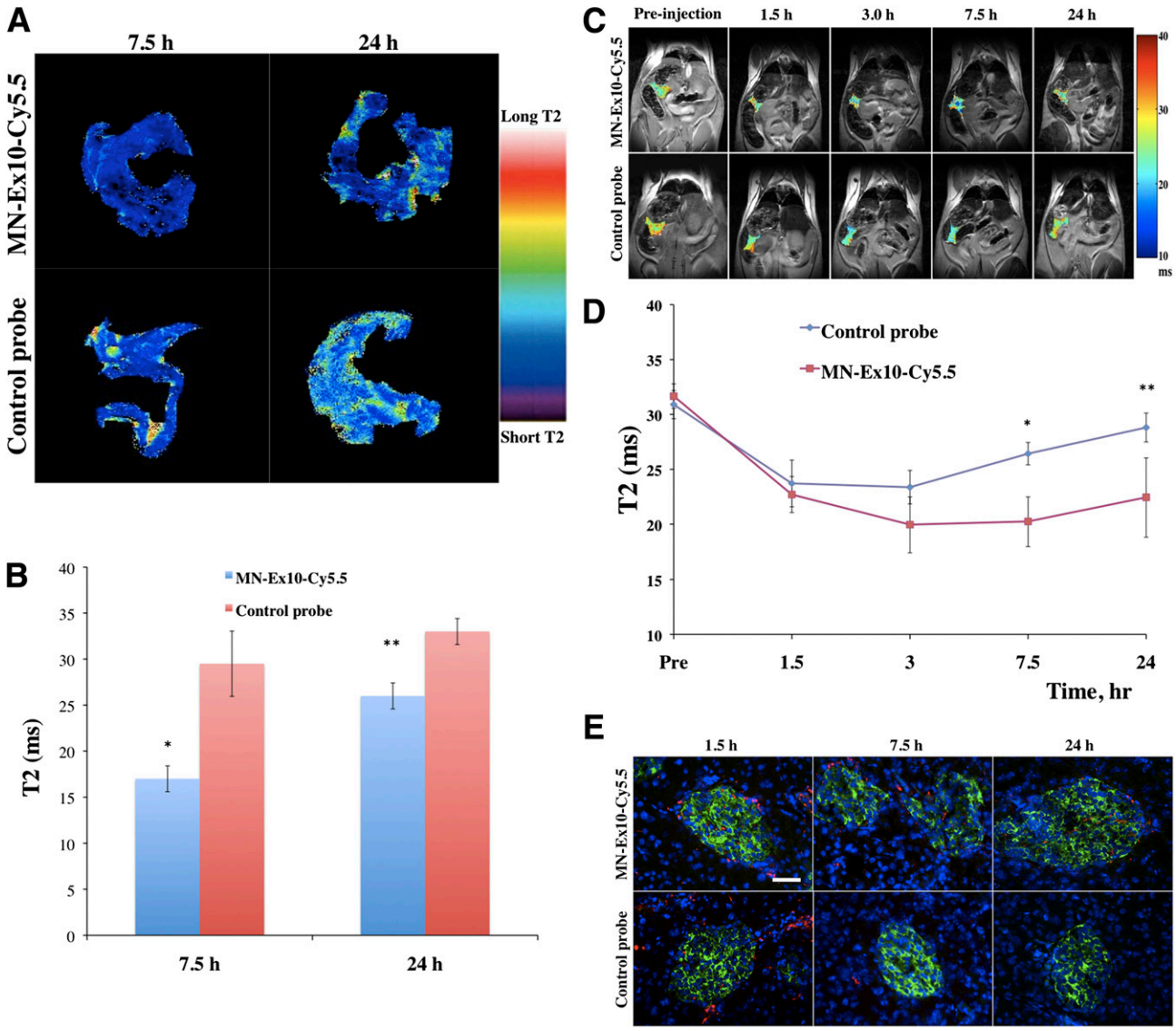

Figure 3—T2-weighted MRI of MN-Ex10-Cy5.5 accumulation in healthy pancreata. *A*: Color-coded T2 map images of the pancreata from mice injected with MN-Ex10-Cy5.5 or control probes. *B*: Quantitative analysis of T2 maps shows significant differences in T2 relaxation times of the pancreata of animals injected with MN-Ex10-Cy5.5 or control probes at 7.5 h (*$P < 0.05$) and 24 h (**$P < 0.05$) after injection. *C*: Coronal T2 maps of healthy mice obtained before and at 1.5, 3, 7.5, and 24 h after injection of MN-Ex10-Cy5.5 or control probes (10 mg Fe/kg). The ROIs of pancreata were color-coded by their T2 relaxation times. Note the decrease in signal intensity after injection of the contrast agent. *D*: Time course quantitative analysis of T2 in the pancreata of mice injected with MN-Ex10-Cy5.5 or control probes. There was a significant difference in T2 relaxation times of the pancreata of animals injected with MN-Ex10-Cy5.5 or control probes at 7.5 h (*$P <$ 0.05) and 24 h (**$P < 0.05$) after injection. *E*: Histochemical immunostaining of the pancreata. MN-Ex-Cy5.5 probe accumulated in β-cells at 1.5, 7.5, and 24 h after intravenous injection. Control MN-Cy5.5 probe showed negligible accumulation in the islets. Cy5.5 (red), insulin (green), and DAPI (blue); magnification bar = 40 μm.

studies on in vivo imaging of transplanted islets labeled with nonspecific iron oxide nanoparticles, we observed an overall shortening of T2 but were not able to separate a single islet structure (45,46). This task became even more challenging when iron oxide–labeled islet grafts were transplanted in nonhuman primates and imaging was performed using low-field clinical scanners (47). In the current study, we observed significant heterogeneities of the signal were especially pronounced on color-coded T2-weighted and T2*-weighted 3D images, reflecting scatter-like distribution of the islets in the pancreas.

The mechanism of nanoparticle accumulation in the pancreas reflects active (target-specific) and passive (vascular) passage. Pancreatic islets are known for their high vascular supply and increased gaps in the endothelium (48), which become significantly more leaky with diabetes development. As suggested by the prior literature, iron oxide nanoparticles were used to detect vascular leakage in association with insulitis in murine models and in patients with T1D (49–51). These studies implied that these particles could migrate from the leaky vessels into the surrounding tissue where they were phagocytosed by

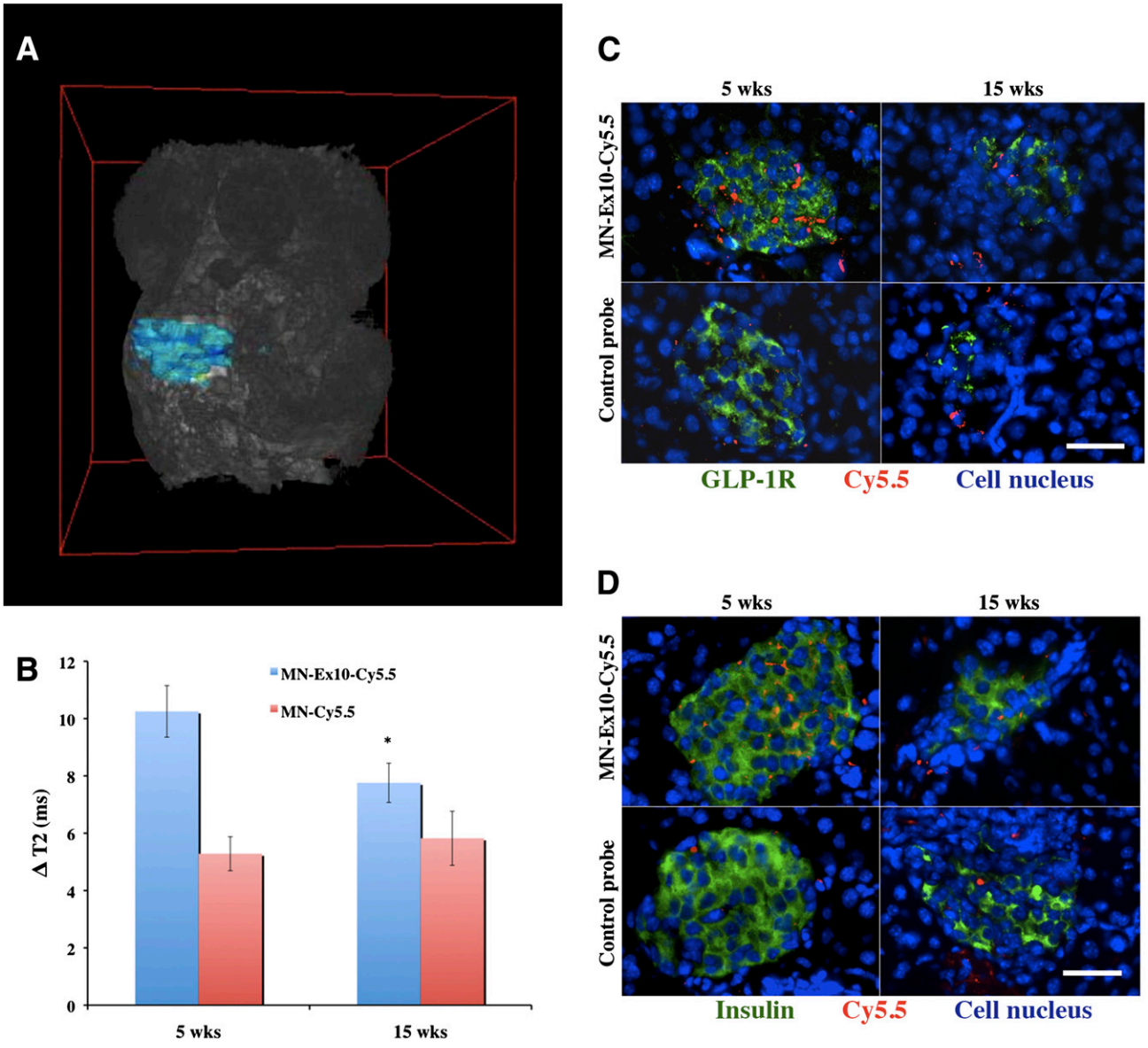

Figure 4—T2-weighted MRI in NOD mice. *A*: Representative 3D T2*-weighted MRI of a 5-week-old NOD mouse shows pancreatic area used for analysis. *B*: The ΔT2 of the pancreata of 15-week-old mice injected with MN-Ex10-Cy5.5 was significantly decreased (*$P < 0.05$) compared with that of 5-week-old NOD mice. *C*: Anti–GLP-1R immunostaining of the pancreata from prediabetic and diabetic NOD mice injected with MN-Ex-Cy5.5 or control probes. Cy5.5 (red), GLP-1R (green), DAPI nuclear stain (blue); magnification bar = 20 μm. *D*: Anti-insulin immunostaining of the pancreata from prediabetic and diabetic NOD mice injected with MN-Ex-Cy5.5 or control probes. Cy5.5 (red), insulin (green), and DAPI nuclear stain (blue); magnification bar = 20 μm. wks, weeks.

inflammatory cells. Indeed, our competition assay results showed that the peptide could not fully abolish the uptake of the probe, indicating the existence of passive phago/macropinocytosis in cultured cells. The results of in vivo MRI also indicate that the tendency for ΔT2 increase with diabetes development in mice injected with the control probe implies the existence of passive uptake in the inflamed tissue. However, the differences in ΔT2 between diabetic mice and prediabetic or healthy mice injected with the control probe were not statistically significant (Fig. 4*B*). In mice injected with MN-Ex-Cy5.5, active targeting by endocytosis was the dominant uptake process and resulted in significant ΔT2 decrease due to the loss of β-cells (Fig. 4*B*). Several studies also showed that GLP-1R expression in β-cells would decrease during hyperglycemia condition (52), which might also contribute to the decrease in ΔT2 between prediabetic and diabetic mice. We need to emphasize that unlike the control probe, MN-Ex10-Cy5.5 resolved the difference in β-cell mass in these animals, pointing to the potential for using this agent for monitoring the disease development and response to therapy.

Iron oxide nanoparticles are a class of medical materials that are particularly well suited for biomedical applications.

They are sized between 10 and 100 nm, and their biodegradable and biocompatible nature makes them suitable for a wide variety of clinical contexts. Currently, several iron oxide nanoparticle–based agents are on the market as MRI contrast probes or for iron supplementation. The key advantage of using nanoparticles is the possibility of loading them with multiple copies of ligand molecules for the targeting of specific tissues (53). More important, these nanoparticles are capable of carrying therapeutic cargo, which makes them even more attractive for theranostic imaging applications. We have already demonstrated suitability of prototype nanoparticles for nucleic acid–based therapy in cancer (54–56) and in the context of islet transplantation (29,30,57). Our intention is to apply similar strategies in the future for therapeutic targeted delivery to endogenous pancreatic islets.

Funding. This work was partly supported by a JDRF award (JDRF 37-2009-30) to A.M. and through the Harvard/Massachusetts General Hospital Nuclear Medicine Training Program funded by the U.S. Department of Energy (DE-SC0008430).

Duality of Interest. No potential conflicts of interest relevant to this article were reported.

Author Contributions. P.W. performed the in vitro experiments, MRI scanning, ex vivo histology staining, and participated in writing the manuscript. B.Y. synthesized the probe. J.Y. participated in MRI data analysis. X.Z. assisted with optical imaging. A.R., P.P., and G.D. researched the data. A.M. conceived the idea of the project and wrote the manuscript. A.M. is the guarantor of this work and, as such, had full access to all the data in the study and takes responsibility for the integrity of the data and the accuracy of the data analysis.

References

1. Mukai E, Toyoda K, Kimura H, et al. GLP-1 receptor antagonist as a potential probe for pancreatic beta-cell imaging. Biochem Biophys Res Commun 2009;389:523–526
2. Mathis D, Vence L, Benoist C. beta-Cell death during progression to diabetes. Nature 2001;414:792–798
3. Fu W, Wojtkiewicz G, Weissleder R, Benoist C, Mathis D. Early window of diabetes determinism in NOD mice, dependent on the complement receptor CRIg, identified by noninvasive imaging. Nat Immunol 2012;13:361–368
4. Wang P, Moore A. Translational molecular imaging of diabetes. Curr Radiol Rep 2013;1:205–215
5. Andralojc K, Srinivas M, Brom M, et al. Obstacles on the way to the clinical visualisation of beta cells: looking for the Aeneas of molecular imaging to navigate between Scylla and Charybdis. Diabetologia 2012;55:1247–1257
6. Nauck MA, Kleine N, Orskov C, Holst JJ, Willms B, Creutzfeldt W. Normalization of fasting hyperglycaemia by exogenous glucagon-like peptide 1 (7-36 amide) in type 2 (non-insulin-dependent) diabetic patients. Diabetologia 1993;36:741–744
7. Rachman J, Gribble FM, Barrow BA, Levy JC, Buchanan KD, Turner RC. Normalization of insulin responses to glucose by overnight infusion of glucagon-like peptide 1 (7-36) amide in patients with NIDDM. Diabetes 1996;45:1524–1530
8. Kim TH, Jiang HH, Lee S, et al. Mono-PEGylated dimeric exendin-4 as high receptor binding and long-acting conjugates for type 2 anti-diabetes therapeutics. Bioconjug Chem 2011;22:625–632
9. Reiner T, Kohler RH, Liew CW, et al. Near-infrared fluorescent probe for imaging of pancreatic beta cells. Bioconjug Chem 2010;21:1362–1368
10. Reiner T, Thurber G, Gaglia J, et al. Accurate measurement of pancreatic islet beta-cell mass using a second-generation fluorescent exendin-4 analog. Proc Natl Acad Sci U S A 2011;108:12815–12820
11. Wang Y, Lim K, Normandin M, Zhao X, Cline GW, Ding YS. Synthesis and evaluation of [18F]exendin (9-39) as a potential biomarker to measure pancreatic β-cell mass. Nucl Med Biol 2012;39:167–176
12. Selvaraju RK, Velikyan I, Johansson L, et al. In vivo imaging of the glucagonlike peptide 1 receptor in the pancreas with ^{68}Ga-labeled DO3A-exendin-4. J Nucl Med 2013;54:1458–1463
13. Pattou F, Kerr-Conte J, Wild D. GLP-1-receptor scanning for imaging of human beta cells transplanted in muscle. N Engl J Med 2010;363:1289–1290
14. Wu Z, Todorov I, Li L, et al. In vivo imaging of transplanted islets with ^{64}Cu-DO3A-VS-Cys40-Exendin-4 by targeting GLP-1 receptor. Bioconjug Chem 2011;22:1587–1594
15. Wu Z, Liu S, Hassink M, et al. Development and evaluation of ^{18}F-TTCO-Cys40-Exendin-4: a PET probe for imaging transplanted islets. J Nucl Med 2013;54:244–251
16. Wild D, Béhé M, Wicki A, et al. [Lys40(Ahx-DTPA-^{111}In)NH2]exendin-4, a very promising ligand for glucagon-like peptide-1 (GLP-1) receptor targeting. J Nucl Med 2006;47:2025–2033
17. Christ E, Wild D, Forrer F, et al. Glucagon-like peptide-1 receptor imaging for localization of insulinomas. J Clin Endocrinol Metab 2009;94:4398–4405
18. Wild D, Wicki A, Mansi R, et al. Exendin-4-based radiopharmaceuticals for glucagonlike peptide-1 receptor PET/CT and SPECT/CT. J Nucl Med 2010;51:1059–1067
19. Kiesewetter DO, Gao H, Ma Y, et al. ^{18}F-radiolabeled analogs of exendin-4 for PET imaging of GLP-1 in insulinoma. Eur J Nucl Med Mol Imaging 2012;39:463–473
20. Kiesewetter DO, Guo N, Guo J, et al. Evaluation of an [(18)F]AlF-NOTA Analog of Exendin-4 for imaging of GLP-1 receptor in insulinoma. Theranostics 2012;2:999–1009
21. Sowa-Staszczak A, Pach D, Mikołajczak R, et al. Glucagon-like peptide-1 receptor imaging with [Lys40(Ahx-HYNIC- ^{99m}Tc/EDDA)NH2]-exendin-4 for the detection of insulinoma. Eur J Nucl Med Mol Imaging 2013;40:524–531
22. Zhang B, Yang B, Zhai C, Jiang B, Wu Y. The role of exendin-4-conjugated superparamagnetic iron oxide nanoparticles in beta-cell-targeted MRI. Biomaterials 2013;34:5843–5852
23. Lunov O, Zablotskii V, Syrovets T, et al. Modeling receptor-mediated endocytosis of polymer-functionalized iron oxide nanoparticles by human macrophages. Biomaterials 2011;32:547–555
24. Duncan R, Richardson SC. Endocytosis and intracellular trafficking as gateways for nanomedicine delivery: opportunities and challenges. Mol Pharm 2012;9:2380–2402
25. Tornehave D, Kristensen P, Rømer J, Knudsen LB, Heller RS. Expression of the GLP-1 receptor in mouse, rat, and human pancreas. J Histochem Cytochem 2008;56:841–851
26. Szot GL, Koudria P, Bluestone JA. Murine pancreatic islet isolation. J Vis Exp 2007:255
27. Zmuda EJ, Powell CA, Hai T. A method for murine islet isolation and subcapsular kidney transplantation. J Vis Exp 2011:2096.
28. Medarova Z, Evgenov NV, Dai G, Bonner-Weir S, Moore A. In vivo multimodal imaging of transplanted pancreatic islets. Nat Protoc 2006;1:429–435
29. Wang P, Yigit MV, Medarova Z, et al. Combined small interfering RNA therapy and in vivo magnetic resonance imaging in islet transplantation. Diabetes 2011;60:565–571
30. Wang P, Yigit MV, Ran C, et al. A theranostic small interfering RNA nanoprobe protects pancreatic islet grafts from adoptively transferred immune rejection. Diabetes 2012;61:3247–3254
31. Jin CH, Chae SY, Son S, et al. A new orally available glucagon-like peptide-1 receptor agonist, biotinylated exendin-4, displays improved hypoglycemic effects in db/db mice. J Control Release 2009;133:172–177
32. Chae SY, Choi YG, Son S, Jung SY, Lee DS, Lee KC. The fatty acid conjugated exendin-4 analogs for type 2 antidiabetic therapeutics. J Control Release 2010;144:10–16

33. Wunderbaldinger P, Josephson L, Weissleder R. Crosslinked iron oxides (CLIO): a new platform for the development of targeted MR contrast agents. Acad Radiol 2002;9(Suppl. 2):S304–S306
34. Moore A, Medarova Z, Potthast A, Dai G. In vivo targeting of underglycosylated MUC-1 tumor antigen using a multimodal imaging probe. Cancer Res 2004;64:1821–1827
35. Moore A, Marecos E, Bogdanov A Jr, Weissleder R. Tumoral distribution of long-circulating dextran-coated iron oxide nanoparticles in a rodent model. Radiology 2000;214:568–574
36. Bourrinet P, Bengele HH, Bonnemain B, et al. Preclinical safety and pharmacokinetic profile of ferumoxtran-10, an ultrasmall superparamagnetic iron oxide magnetic resonance contrast agent. Invest Radiol 2006;41:313–324
37. Ban K, Noyan-Ashraf MH, Hoefer J, Bolz SS, Drucker DJ, Husain M. Cardioprotective and vasodilatory actions of glucagon-like peptide 1 receptor are mediated through both glucagon-like peptide 1 receptor-dependent and -independent pathways. Circulation 2008;117:2340–2350
38. Kedees MH, Guz Y, Grigoryan M, Teitelman G. Functional activity of murine intestinal mucosal cells is regulated by the glucagon-like peptide-1 receptor. Peptides 2013;48:36–44
39. Richards P, Parker HE, Adriaenssens AE, et al. Identification and characterization of GLP-1 receptor–expressing cells using a new transgenic mouse model. Diabetes 2014;63:1224–1233
40. Arifin DR, Bulte JW. Imaging of pancreatic islet cells. Diabetes Metab Res Rev 2011;27:761–766
41. Antkowiak PF, Stevens BK, Nunemaker CS, McDuffie M, Epstein FH. Manganese-enhanced magnetic resonance imaging detects declining pancreatic β-cell mass in a cyclophosphamide-accelerated mouse model of type 1 diabetes. Diabetes 2013;62:44–48
42. Lubag AJ, De Leon-Rodriguez LM, Burgess SC, Sherry AD. Noninvasive MRI of β-cell function using a Zn2+-responsive contrast agent. Proc Natl Acad Sci U S A 2011;108:18400–18405
43. Canton I, Battaglia G. Endocytosis at the nanoscale. Chem Soc Rev 2012;41:2718–2739
44. Yuan H, Li J, Bao G, Zhang S. Variable nanoparticle-cell adhesion strength regulates cellular uptake. Phys Rev Lett 2010;105:138101
45. Evgenov NV, Medarova Z, Dai G, Bonner-Weir S, Moore A. In vivo imaging of islet transplantation. Nat Med 2006;12:144–148
46. Evgenov NV, Medarova Z, Pratt J, et al. In vivo imaging of immune rejection in transplanted pancreatic islets. Diabetes 2006;55:2419–2428
47. Medarova Z, Vallabhajosyula P, Tena A, et al. In vivo imaging of autologous islet grafts in the liver and under the kidney capsule in non-human primates. Transplantation 2009;87:1659–1666
48. Bonner-Weir S. The microvsaculature of the pancreas, with emphasis on that of the islets of langerhans. In *The Pancreas: Biology, Pathobiology, and Disease*. Go VL, DiMagno EP, Gardner JD, Lebenthal E, Reber HA, Scheele GA, Eds. New York, Raven Press, 1993, p. 759–768
49. Denis MC, Mahmood U, Benoist C, Mathis D, Weissleder R. Imaging inflammation of the pancreatic islets in type 1 diabetes. Proc Natl Acad Sci U S A 2004;101:12634–12639
50. Turvey SE, Swart E, Denis MC, et al. Noninvasive imaging of pancreatic inflammation and its reversal in type 1 diabetes. J Clin Invest 2005;115:2454–2461
51. Gaglia JL, Guimaraes AR, Harisinghani M, et al. Noninvasive imaging of pancreatic islet inflammation in type 1A diabetes patients. J Clin Invest 2011;121:442–445
52. Xu G, Kaneto H, Laybutt DR, et al. Downregulation of GLP-1 and GIP receptor expression by hyperglycemia: possible contribution to impaired incretin effects in diabetes. Diabetes 2007;56:1551–1558
53. Jokerst JV, Gambhir SS. Molecular imaging with theranostic nanoparticles. Acc Chem Res 2011;44:1050–1060
54. Medarova Z, Pham W, Farrar C, Petkova V, Moore A. In vivo imaging of siRNA delivery and silencing in tumors. Nat Med 2007;13:372–377
55. Kumar M, Yigit M, Dai G, Moore A, Medarova Z. Image-guided breast tumor therapy using a small interfering RNA nanodrug. Cancer Res 2010;70:7553–7561
56. Yigit MV, Ghosh SK, Kumar M, et al. Context-dependent differences in miR-10b breast oncogenesis can be targeted for the prevention and arrest of lymph node metastasis. Oncogene 2013;32:1530–1538
57. Medarova Z, Kumar M, Ng SW, et al. Multifunctional magnetic nanocarriers for image-tagged SiRNA delivery to intact pancreatic islets. Transplantation 2008;86:1170–1177